SUPPLEMENT TO THE *WELDING JOURNAL*, JANUARY 2012
Sponsored by the American Welding Society and the Welding Research Council

Ultrasonic Soldering of Shape Memory NiTi to Aluminum 2024

Shape memory alloy and aluminum joints were soldered with a fluxless process and analyzed for strength and hardness

BY R. HAHNLEN, G. FOX, AND M. DAPINO

ABSTRACT

Nickel-titanium (NiTi) shape memory alloys can recover up to 8% induced strain, allowing these alloys to be used in solid-state actuation. However, the implementation of NiTi in structural applications can be expensive, complex, and in some cases unfeasible due to limitations of traditional joining techniques. This research investigates joining of NiTi and Al 2024 by ultrasonic soldering (USS), a process that can solder difficult to wet materials without the use of flux. The USS joints were evaluated through lap shear and torsional shear strength testing, optical microscopy, hardness testing, and maximum calculated von Mises equivalent stresses developed during manufacturing and testing. Lap shear tests have an average ultimate shear stress of 7.80 ksi (53.8 MPa) while torsion joints have an average ultimate shear stress of 5.35 ksi (36.9 MPa). Hardness testing shows that while the bulk NiTi is unaffected by the USS process, there is a narrow region of increased hardness believed to be due to alloying with the filler metal.

Introduction

Shape memory alloys are a class of smart materials that can be plastically deformed and then recover their original shape upon heating above the material's austenitic finish temperature. Nickel-titanium (NiTi) is a particular shape memory alloy that can be strained up to 8% and fully recover all this deformation (Ref. 1) via temperature-induced phase tranfsormation between martensite and austenite. Although NiTi actuators can in some cases replace large, heavy motors, there are several critical issues in machining and joining NiTi to structural materials, which make it difficult to integrate NiTi actuators into structural applications.

Machining of NiTi alloys has proven to be difficult due to the high ductility, work hardening characteristics, and the nonlinear stress-strain behavior of these alloys. These characteristics can cause poor surface finish, irregular chip breakage, and high tool wear (Ref. 2). The buildup of heat in traditional machining processes can also locally affect thermomechanical properties of the NiTi workpiece (Ref. 3). Processes such as laser machining and electric discharge machining are commonly used to create NiTi parts, though these processes are relatively expensive when compared to traditional machining processes. Much of the expense of using NiTi can be eliminated if a reliable and efficient way of joining it to traditional structural materials, such as aluminum alloys, is found; however, joining NiTi to itself and dissimilar materials presents several challenges.

Although fusion welding processes are commonly used for joining metal parts, there are several concerns in fusion welding NiTi both to itself and to dissimilar metals. NiTi components obtain their repeatable shape memory and superelastic behaviors through stabilization of the crystalline structure and dislocation networks as governed by material training through repeated loading cycles and cold work. In the welding process, the high temperatures nullify the training through grain growth and recrystalization. While the original behaviors can be partially recovered through a combination of heat treatment and additional training, this adds complexity and cost to the joining process due to the additional processing steps (Ref. 4). Fusion welding NiTi to dissimilar materials is also difficult due the formation of intermetallics, which cause cracks to propagate during cooling (Ref. 5).

Soldering is a more desirable option for creating joints containing NiTi as it involves no melting of the base metal and the filler metal melts at or below 450°C (Refs. 6, 7). The relatively low temperatures in soldering processes avoid degradation of the shape memory and superelastic properties of the NiTi components. The main obstacle in creating NiTi-containing solder joints is in wetting the surface of the NiTi with the solder. The tenacious surface oxides that form on the surface of Ti and its alloys usually require the use of harsh surface treatments and aggressive fluxes (Refs. 8, 9). The use of flux raises concerns including the increased complexity of an additional process step, waste disposal, and health concerns for those working with fluxes, as well as issues with corrosion if flux residue is not completely removed from finished joints (Ref. 7).

This research investigates the use of ultrasonic soldering (USS), a fluxless process for creating joints between NiTi and aluminum 2024 (Al 2024). Ultrasonic soldering is able to solder difficult to wet materials through two mechanisms: a reactive element in the solder alloy and mechanical disruption of the base metal surface oxides. The solder used for this research employed Al as the active element, which improved wetting by reacting with the base metal and its surface oxides (Refs. 8, 10, 11). The mechanical disruption of the surface oxides is provided by ul-

KEYWORDS

Ultrasonic Soldering
Memory Alloys
Soldering
NiTi
Aluminum

R. HAHNLEN, G. FOX, AND M. DAPINO are with Smart Vehicle Concepts Center, Department of Mechanical and Aerospace Engineering, The Ohio State University, Columbus, Ohio.

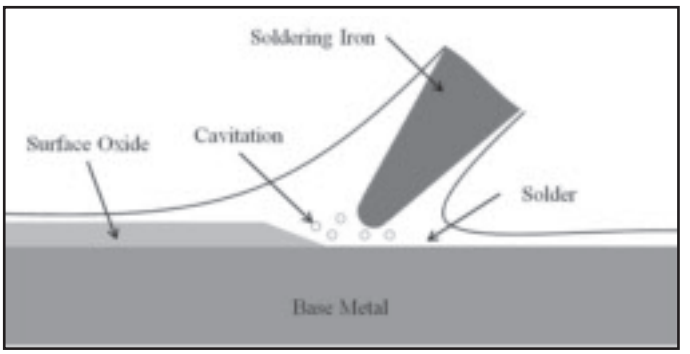

Fig. 1 — Schematic representation of the ultrasonic soldering (USS) process.

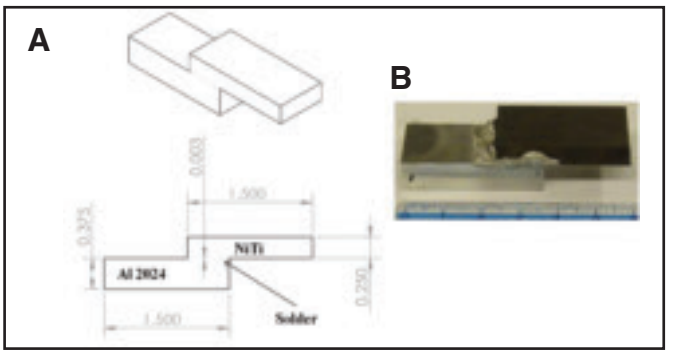

Fig. 2 — A — Diagram of USS lap shear specimen; B — USS NiTi/Al2024 lap shear joint.

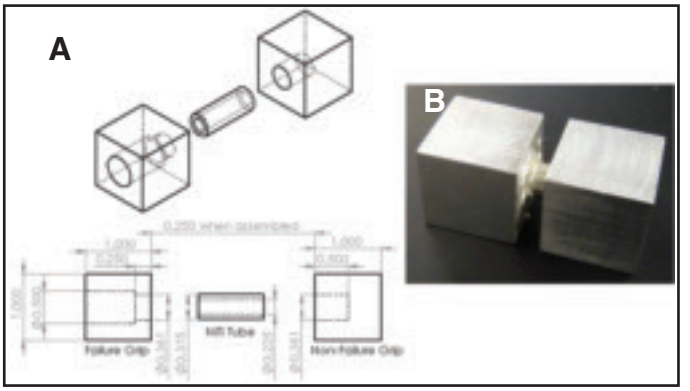

Fig. 3 — A — Schematic of USS tube and socket torsional testing sample; B — USS tube and socket torsional sample.

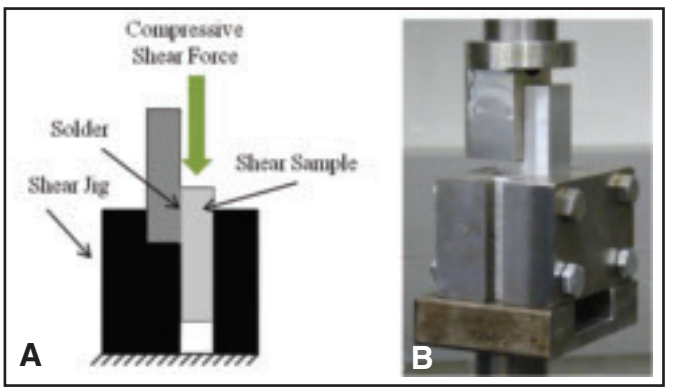

Fig. 4 — A — Diagram of compressive shear test jig; B — shear test setup.

trasonic vibrations of a soldering iron tip created by a piezoelectric transducer. When tinning the faying surfaces, the ultrasonic vibrations create cavitations in the liquid solder resting on the base metal. As the cavitations implode, they impinge upon the surface of the base metal breaking up surface oxide layers and cleaning the faying surface, as shown in Fig. 1. The combination of the active solder element and mechanical removal of surface oxides decreases the contact angle between the solder and faying surface (Ref. 7) thus allowing the solder to wet otherwise not-wetting materials such as ceramics, glass, titanium, and aluminum without the use of flux (Ref. 8).

This paper discusses the construction, testing, and analysis of lap shear and torsional shear NiTi/Al 2024 USS joints. Al 2024 was chosen because it is a common aerospace alloy noted for its fatigue strength and moderately high yield strength (Ref. 12). Lap shear joints are used as a preliminary evaluation of the process while torsional tube and socket-based joints are studied to represent the type of joint that would be used in a NiTi torsional actuator. Joints are evaluated through mechanical strength testing, optical microscopy, and hardness testing. Lastly, the complex state of stress due to the manufacturing process and mechanical loading is analyzed.

Table 1 — NiTi/Al 2024 Lap Shear Test Results

Sample	Ultimate Shear Strength ksi (MPa)
1	7.52 (51.8)
2	8.37 (57.7)
3	7.51 (51.8)
Average	7.80 (53.8)
Standard Deviation	0.49 (3.4)
C_v	6.3%

Table 2 — NiTi/Al 2024 Torsional Test Results

Sample	Torque in.-lb (N-m)	Ultimate Shear Stress ksi (MPa)
1	282 (31.9)	5.11 (35.2)
2	288 (32.5)	5.22 (35.9)
3	284 (32.1)	5.14 (35.4)
4	297 (33.6)	5.38 (37.1)
5	327 (37.0)	5.92 (40.8)
Average	296 (33.4)	5.35 (36.9)
Standard Deviation	18.5 (2.1)	0.33 (2.3)
C_v		6.2%

Experimental Methods

Sample Construction

A lap shear joint is the typical geometry used for load-bearing solder, braze, and adhesive joints (Refs. 6, 7, 13). In this geometry, the joint area can be easily increased to augment joint strength. Unlike a solder joint in tension, the strength of a soldered lap shear joint is not strongly dependent on the thickness of the solder layer (Ref. 14).

Prior to soldering any joints, each workpiece was first given a surface preparation consisting of a 50-μm SiC grit blast of all faying surfaces followed by a methanol rinse to remove any SiC particles and other surface contaminants. Previous research has shown that this particular surface treatment creates stronger and more consistent USS joints when compared to nonsurface-treated USS joints (Ref. 15).

During soldering of the lap shear specimens, base metal pieces were placed on a

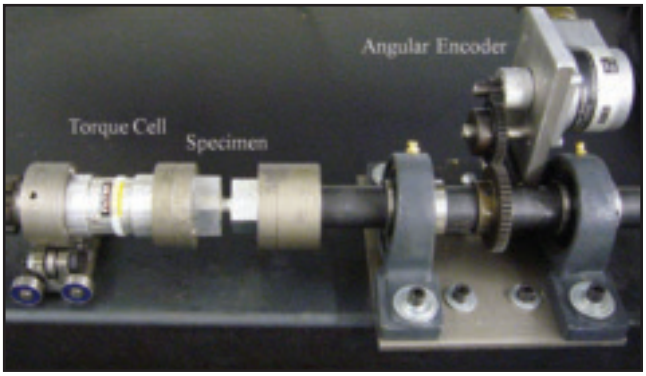

Fig. 5 — Torsional testing setup.

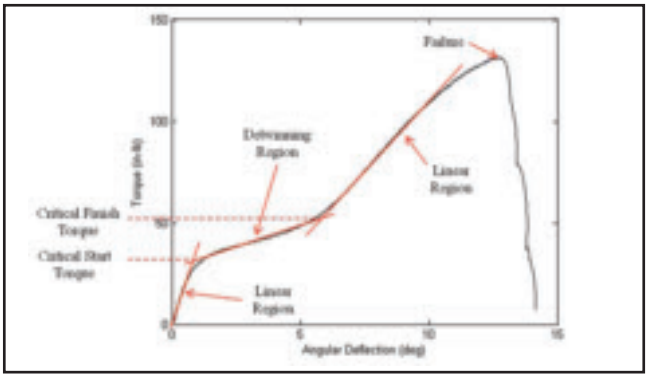

Fig. 6 — Torque-angle plot of a thin-walled NiTi tube displaying critical torque loads and failure.

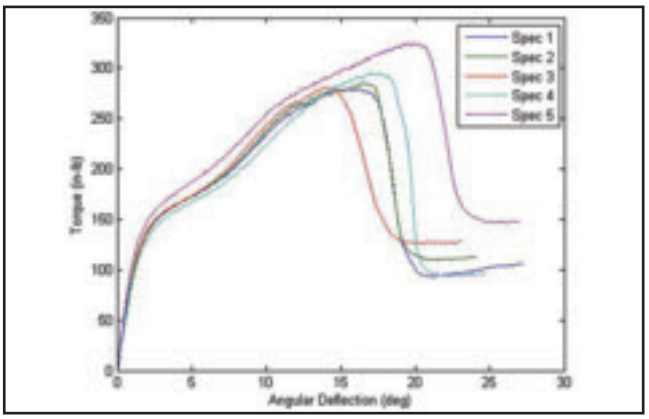

Fig. 7 — Torque-angle plots of NiTi/Al 2024 USS torsion joints.

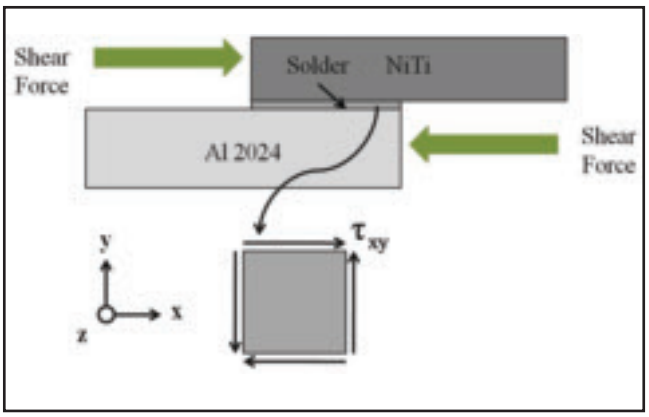

Fig. 8 — Differential solder element in USS lap shear joints.

hot plate and preheated to 250°C, approximately 20°C above the melting point of the filler metal (Ref. 10), to ensure that the solder was fully melted and to allow for cavitation. The faying surfaces were next tinned using a USS iron with a flat tip. Once tinned, the base metals were placed on a soldering jig, which was designed to maintain a nominal solder thickness of 0.003 in. (0.08 mm). Additional solder was placed at the joint interface in order to fill any voids by capillary action and to ensure a consistent, void-free, solder joint. After assembly, the jig and sample were taken from the hot plate and allowed to cool.

The USS lap shear specimens were constructed using Al 2024 pieces 0.375 in. (9.53 mm) thick, 0.675 in. (17.2 mm) wide and 1.500 in. (38.10 mm) long. The NiTi pieces (55 wt-% Ni) used were 0.250 in. (6.35 mm) thick. The workpieces were soldered such that a joint area of 0.675 × 0.500 in. (17.2 × 12.7 mm) was created. Figure 2A shows a typical shear test specimen with nominal thickness dimensions. After soldering, samples were machined to remove solder flash. Figure 2B shows a NiTi/Al 2024 lap shear sample before solder flash removal.

Five tube-and-socket torsional joints were created using NiTi tubes and Al 2024 blocks. The tubes had an outer diameter of 0.375 in. (9.53 mm), an inner diameter of 0.225 in. (5.72 mm), and a nominal length of 1.00 in. (25.4 mm). One of the grips was designed to fail during the test by having half the bonded area of the other grip. The grip that was designed to fail had a through-hole with a radius 0.003 in. (0.08 mm) larger than the NiTi tube radius for the first 0.250 in. (6.35 mm) of depth, then much larger for the rest of the depth. The other grip had a blind hole with a radius 0.003 in. (0.08 mm) larger than the radius of the NiTi tube, with a depth of 0.500 in. (12.7 mm). When assembled, the faces of the two grips were nominally 0.250 in. (6.35 mm) apart. This geometry is shown in Fig. 3A.

Both NiTi tubes and Al 2024 blocks were subject to a 50-μm SiC grit blast and rinsed with methanol prior to being soldered. Similar to the lap shear joints, the tube and blocks were heated to 250°C, and then tinned with an ultrasonic soldering iron with curved tips. A concave tip was used to wet the surface of the NiTi tube, and a convex tip for the holes in the Al 2024 blocks. The three pieces were assembled and then allowed to cool. Once cooled, excess solder was filed off of the NiTi tube between the grip faces. A photograph of an assembled joint is shown in Fig. 3B.

Table 3 — Material Properties Used to Calculate Thermally Induced Stresses in Lap Shear Joints

Material	NiTi	Al 2024
t in. (mm)	0.250 (6.350)	0.375 (9.525)
α με/°C	10 [Ref. 17]	23.2 [Ref. 18]
E ksi (MPa)	3770 (26000) [Ref. 19]	9860 (68000) [Ref. 18]

Sample Testing

Shear tests of the lap joints utilized a testing jig that supports one base metal while applying a direct shear load to the other base metal as shown in Fig. 4. This loading method causes all resulting shear stresses to be transmitted through the solder joint. Test specimens were loaded in compression under displacement control

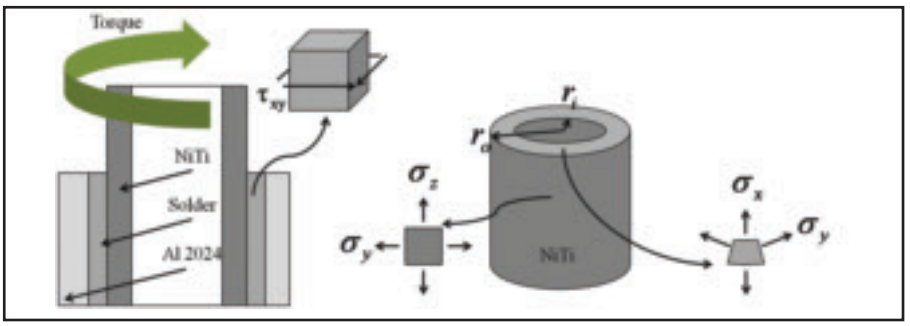

Fig. 9 — Differential solder element in USS torsion joint.

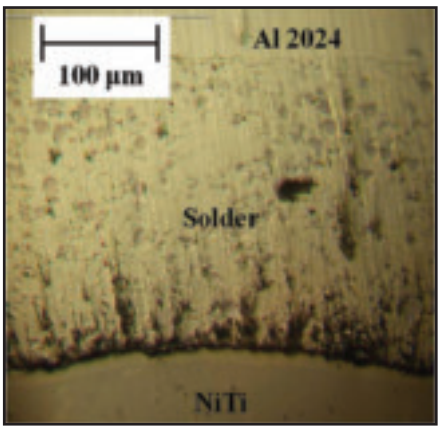

Fig. 10 — USS NiTi/Al 2024 USS lap joint cross section.

until failure by applying a ramp input with a rate of 0.010 in./s (0.25 mm/s). During testing, ram displacement was measured by an LVDT integrated in the load frame and the applied force was measured using a load cell placed in series with the load train.

The tube and socket specimens were tested to failure in a torsional testing machine at an angular velocity of approximately 0.5 deg/s. The failure torque was the maximum torque measured during the test. A torsion test of a sample can be seen in Fig. 5. During testing, applied torque was measured with a reaction torque cell while angular displacement was measured with an angular encoder.

USS Sample Sectioning

One NiTi/Al 2024 USS joint was constructed for the purpose of mounting, sectioning, and polishing to observe the interface of the NiTi sample and Al 2024 with the filler metal. The Al 2024 sample was machined with a 0.003-in. (0.08-mm) recess to control solder thickness. Faying surfaces of the NiTi and Al 2024 pieces were treated with a 50-µm SiC grit blast and methanol rinse prior to joining. The resulting joint was cold mounted in an epoxy matrix.

After optical microscopy observations were made, a hardness map was created of the NiTi portion of the joint to investigate the presence of an affected zone. The map was created by making an array of indents with a 100-g (3.53-oz) load spaced 200 µm (0.008 in.) in both the x and y axes of the cold-mounted sample cross section. After the map was created, individual hardness tests were conducted at points of interest with a 10-g (0.35-oz) load. These individual points were identified through optical microscopy. Vickers hardness was used to evaluate the sample map and individual points.

Results and Discussion

Lap Shear and Torsional Shear Results

Table 1 shows the ultimate shear stress for NiTi/Al 2024 lap shear joints. The average strength for these measurements is 7.80 ksi (53.8 MPa) with a coefficient of variance, $C_v = \bar{s}/\tau$ where s is the standard deviation and τ is the average ultimate shear strength of 6.3%.

The failure torque and average shear stress for the torsion joints are presented in Table 2. After failure, the torque did not drop to zero, but instead to approximately 89 in.-lb (10 N-m) where it remained constant with increasing rotation. This is due to friction between the failure surfaces that remain in contact due to the geometry of the joint.

The shear stress at the interface between the NiTi tube and solder is calculated from the torque, of T, by

$$\tau = \frac{2T}{\pi d^2 l} \quad (1)$$

Here, l is the bonded length, and d is the diameter of the joint. For these specimens, l is 0.250 in. (6.35 mm) and d is 0.375 in. (9.53 mm). This calculation treats the solder joint as a thin-walled tube in torsion and assumes that the stress in the solder is uniform through its thickness. Since the outer radius of the NiTi tubes and the radius of the sockets in the Al blocks differ by only 0.003 in. (0.08 mm), the ratio of solder thickness to the radius formed by the cylindrical solder joint is 1/125, less than the ratio of 1/10 commonly required for thin-walled tube analysis (Ref. 16) and validates the use of Equation 1.

Table 4 — Thermally Induced Stresses in Lap Shear Joints

Material	Bending Stress, ksi (Mpa)
Al 2024	–7.79 (–53.71)
NiTi	–0.79 (–5.45)
Solder	–3.59 (–24.75)

Residual Stress Analysis

The USS joints studied have base metals with a large difference in coefficients of thermal expansion (CTEs). In manufacturing the specimens, the solder cools and solidifies, constraining the base metals and solder joint, and then further cools to room temperature. The difference in CTEs causes distortion of the pieces and generates residual stresses as the temperature changes. Since NiTi has a nonlinear stress-strain relationship, the stress generated in the NiTi pieces due to the residual stresses is assumed to be limited to the critical detwinning start stress. At this stress the crystal structure of NiTi begins to change from either twinned martensite or austenite, depending upon temperature, to detwinned martensite. The change in structure takes place in the detwinning plateau, a region of large strain increase for a small stress increase, which is the source of the recoverable strain in shape memory alloys. This is demonstrated in a torque-angle plot, shown in Fig. 6, which was obtained from a thin-walled NiTi specimen. The plot shows an initially elastic region followed by the detwinning plateau indicated by the low-torque-angle slope, followed by a second linear region until failure. The detwinning plateau occurs over a range of torque bounded by the critical start and critical finish torques, i.e., the torque levels required to generate the critical start and critical finish stresses within the NiTi tube. These values are determined by finding the intersections of the extrapolated linear elastic regions and the detwinning plateau, denoted by red lines in Fig. 6.

In NiTi, the strain from thermal expansion is smaller than the strain over the detwinning plateau, commonly observed between 6 and 8% (Ref. 17). As a result, we assume that any residual stress that develops in the NiTi tube due to cooling of the dissimilar base metals reaches a maximum when the stress in the NiTi portion of the joint reaches the critical start stress. Any additional strain is accommodated by the NiTi tube with a small increase in stress due to the detwinning plateau. The

combination of residual stress from manufacturing and mechanical stress from testing creates a complex state of stress within the solder joint. In order to determine the stress in each joint during mechanical testing, the stress developed during cooling is calculated and added to the mechanical stresses applied during testing. The triaxial state of stress is then used to calculate principal stresses and the von Mises equivalent stress for both joint types at failure.

In order to determine the critical start stress, the torque-angle plots for the torsional specimens, shown in Fig. 7, are examined. The beginning of the detwinning plateau is observed in these plots, though the end of detwinning is not as clearly defined as it is for the thin-walled tube. This is because the thicker wall of the NiTi tube has a varying shear stress through its thickness allowing more martensite to detwine near the outer radius of the tube as opposed to the thin-walled tube, which has a nearly uniform shear stress through its wall thickness. The linear intercept method used to find critical torques in Fig. 6 was used on the torque-angle plots in Fig. 7. By finding the intersection of linear extrapolations of the initial elastic region and detwinning plateau, the average critical start torque was determined to be 144.3 in.-lb (16.30 N-m). The critical shear stress can be obtained by using the torsional shear equation,

$$\tau_{\max}^{cr} = \frac{T^{cr} r_o}{J} \tag{2}$$

where

$$J = \frac{\pi}{2}\left(r_o^4 - r_i^4\right) \tag{3}$$

and r_o, r_i, T^{cr} are the outer radius, inner radius, and critical detwinning torque, respectively. For general use of the critical stress, it is transformed into a von Mises equivalent stress where the principal stresses are σ_1, σ_2, $= \pm \tau^{cr}_{,max}$, $\sigma_3 = 0$, and the equivalent stress is given by (Ref. 17)

$$\sigma_{eq} = \sqrt{\frac{1}{2}\left[(\sigma_1 - \sigma_2)^2 + (\sigma_2 - \sigma_3)^2 + (\sigma_3 - \sigma_1)^2\right]} \tag{4}$$

which simplifies to

$$\sigma_{eq} = \sigma_{eq}^{cr} = \sqrt{3}\tau_{\max}^{cr}. \tag{5}$$

The average τ^{cr}_{max} from the five specimens is 16.0 ksi (110 MPa), which corresponds to σ_{eq}=27.7 ksi (191 MPa).

The residual stresses due to differential thermal expansion of the dissimilar base metals are calculated for the NiTi/Al 2024 lap shear USS joints by considering a bimetal system with the two pieces fixed to each other at their mutual interface. The stress in the outer fiber of the Al 2024 component is calculated by (Ref. 16)

$$\sigma_{Al} = \frac{-(\alpha_{NiTi} - \alpha_{Al})(\Delta T)E_{Al}}{K_1}\left[3\frac{t_{Al}}{t_{NiTi}} + 2\left(\frac{t_{Al}}{t_{NiTi}}\right)^2 - \frac{E_{NiTi}t_{NiTi}}{E_{Al}t_{Al}}\right] \tag{6}$$

and the stress in the outer fiber of the NiTi component is given by (Ref. 16)

$$\sigma_{NiTi} = \frac{-(\alpha_{Al} - \alpha_{NiTi})(\Delta T)E_{NiTi}}{K_1}\left[3\frac{t_{Al}}{t_{NiTi}} + 2 - \frac{E_{Al}}{E_{NiTi}}\left(\frac{t_{Al}}{t_{NiTi}}\right)^3\right] \tag{7}$$

where

$$K_1 = 4 + 6\left(\frac{t_{Al}}{t_{NiTi}}\right) + 4\left(\frac{t_{Al}}{t_{NiTi}}\right)^2 + \frac{E_{Al}}{E_{NiTi}}\left(\frac{t_{Al}}{t_{NiTi}}\right)^3 + \frac{E_{NiTi}t_{NiTi}}{E_{Al}t_{Al}} \tag{8}$$

For this analysis, the NiTi piece is treated as a linear elastic material with an elastic modulus equal to its martensitic elastic modulus. Material properties used for calculation of residual stresses are shown in Table 3. The stresses are considered to develop when the joint cools from 231°C, the melting point of the filler metal (Ref. 10), to 20°C.

By assuming a linear stress gradient from the outer fiber of the Al 2024 block and outer fiber of the NiTi piece in each joint and assuming the stress in the solder is equal to the stress at the NiTi/Al interface, the stress at the interface is calculated by interpolating the stress at distance t_{Al} from the outer fiber of the Al 2024:

$$\sigma_{solder} = \sigma_{Al} + t_{Al}\left(\frac{\sigma_{NiTi} - \sigma_{Al}}{t_{Al} + t_{NiTi}}\right) \tag{9}$$

The resulting estimated residual stresses are presented in Table 4.

The thermally induced stress in the NiTi component is smaller than the equivalent detwinning stress, hence the assumption of linear elasticity used to calculate the thermally induced stress is reasonable. Since this thermal stress occurs both in the x direction as oriented in Fig. 8 and the z direction coming out of the page, the stress in the solder can be determined by setting σ_x and σ_z equal to σ_{solder} and τ_{xy} equal to the average ultimate shear strength. This results in principal stresses in the solder joint of σ_1= 6.21 ksi (42.82 MPa), σ_2 = –3.59 ksi (–24.75 MPa), and σ_3 = –9.79 ksi (–67.50 MPa), and von Mises stress of 13.98 ksi (96.39 MPa).

In considering the differential thermal expansion of the Al 2024 and NiTi in the torsional joints, an FEA model was created considering linear elastic materials and a change in temperature from 231° to 20°C. The FEA model suggests that residual stresses generated from the temperature change exceed the critical start stress of NiTi. This indicates that the NiTi tube begins to detwin due to thermally induced stresses and the linear elastic FEA model will over estimate the stresses within the solder.

Stresses were recalculated by modeling the NiTi tube as a thick-walled vessel with

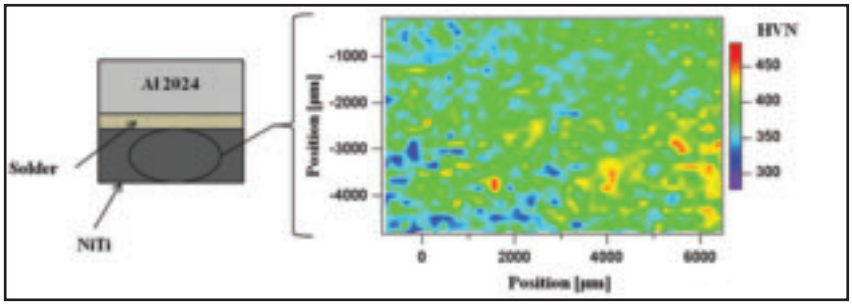

Fig. 11 — Hardness map of NiTi/Al 2024 USS lap joint.

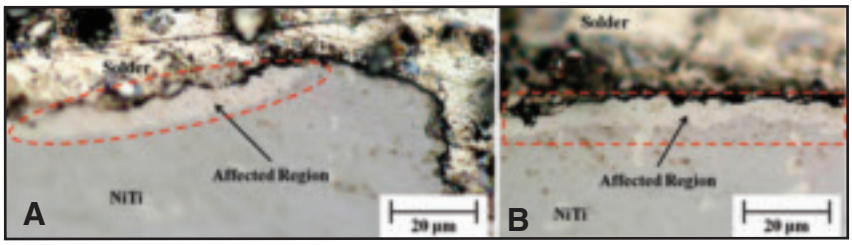

Fig. 12 — Micrographs showing affected region in NiTi. A — Edge of faying surface; B — middle of joint.

external pressure. The associated stresses, σ_x, σ_y, and σ_z, (Fig. 9) can be calculated as follows (Ref. 16):

$$\sigma_x = \frac{-qr_o^2\left(r^2 - r_i^2\right)}{r^2\left(r_o^2 + r_i^2\right)} \quad (10)$$

$$\sigma_y = \frac{-qr_o^2\left(r_i^2 + r^2\right)}{r^2\left(r_o^2 + r_i^2\right)} \quad (11)$$

and

$$\sigma_z = 0 \quad (12)$$

where q is the external pressure, r_o is the outer radius, r_i is the inner radius, and r is the radius. At the solder/NiTi interface, residual stress in the solder layer is the same as residual stress in the outer fiber of the NiTi tube. This is because Equations 10–12 are dependent upon radius and pressure only, both of which are identical for the NiTi and solder at the interface. The nonzero stresses are σ_x and σ_y, which become $-q$ and $-2.126q$, respectively. The principal stresses for the compressed tube are $\sigma_1 = 0$, $\sigma_2 = -q$, and $\sigma_3 = -2.126q$. In order to find the external pressure, q, that causes the NiTi tube to begin detwinning, σ_{eq} from Equation 4 is taken as σ^{cr}_{eq} =27.7 ksi (191.0 MPa). The external pressure required to start detwinning is found to be 15.0 ksi (103.4 MPa). In turn, σ_x and σ_y become –15.0 and –31.9 ksi (–103.4 and –219.9 MPa), respectively.

Using σ_x, σ_y, σ_z, and the average ultimate shear strength of torsion joints as τ_{xy}, the principal stresses are found to be σ_1 = 0 ksi, σ_2 =–13.45 ksi (–92.73 MPa), and σ_3 = –33.45 ksi (–230.6 MPa), which are used to find the von Mises equivalent stress for the torsional joints, 29.15 ksi (201.0 MPa).

USS Sample Sectioning

Figure 10 shows a micrograph of a cold-mounted NiTi/Al 2024 USS joint section. The thickness of the solder is uniform and there is intimate contact between the solder and both base metals. Using this sample section, the hardness map shown in Fig. 11 was created. The average Vickers hardness in the NiTi section was found to be 380 HV with a standard deviation of 30 HV.

Optical microscopy reveals a narrow shaded region extending into the NiTi from the solder joint. The region is observed only on the faying surface of the NiTi and ends at the edges of the joined surface (Fig. 12A) maintaining a consistent depth, which averages 6.4 μm (250 μin.) thick over the entire faying surface — Fig. 12B. The region's thickness is less than the resolution of the hardness map, which motivated individual hardness test points to observe if this region behaves differently than the bulk NiTi. This region is significantly harder than the bulk NiTi observed in the hardness map. Two additional hardness measurements in this affected zone have a hardness of 543 and 571 HV. A hypothesis for the increased hardness is discussed in the following section.

Discussion

Both the lap shear joints and torsional joints had consistent ultimate shear strengths with coefficients of variance of 6.3% and 6.2%, respectively. These results indicate that USS is a robust process capable of creating joints of consistent strength. The lap shear joints had a higher average ultimate shear strength than the torsional shear joints, 7.80 ksi (53.8 MPa) vs. 5.35 ksi (36.9 MPa).

While the ultimate shear stresses in the torsional joints were smaller than the stresses in the lap shear joints, the torsional samples were found to have a higher residual stress, through calculations described previously, resulting from the dissimilar CTEs of Al 2024 and NiTi. When considering the complex state of stress due to mechanical loading and the calculated thermally induced residual stresses, the average equivalent stress in the torsional shear samples at failure was significantly higher than that of the lap shear joints, 29.15 ksi (201.0 MPa) vs. 13.98 ksi (96.39 MPa). This indicates that the residual stresses due to joint construction are dependent upon joint geometry and can add a significant portion to the total stress in the solder joint. The analysis presented previously provides an estimation of the residual stresses resulting from the USS process in both samples. Future analyses will be focused on obtaining refined von Mises stress values through more rigorous models incorporating the nonlinear stress-strain behavior of NiTi.

The average hardness of the bulk NiTi in the USS cross section is typical of NiTi alloys as is the minor variation in hardness measurements (Ref. 20). The deviation is likely due to different orientations of the martensite phase of the NiTi, which would result in different indent sizes due to varying amounts of transformation strain occurring at the test points as the indenter deforms the base material.

While the bulk NiTi was found to be unaffected by the joining process, the shaded region identified through microscopy displays a significant increase in hardness of NiTi immediately adjacent to the solder. Since the NiTi piece is at a relatively low process temperature for a few minutes during the joining process, it is not believed that this increase in hardness is due to a heat-affected zone (HAZ). Further, the soldering iron is maintained at the same temperature as the hot plate, so any HAZ would be noticeable in the bulk NiTi as well as the faying surface. It is hypothesized that the region observed near the faying surface is an alloy zone where constituents of the filler metal have diffused into the NiTi piece during the soldering process and alloyed with the base metal.

The temperatures of the joining process would appear to be too low to support diffusion and alloying at the joining time scale; however, with the addition of the ultrasonically vibrating soldering iron, diffusion may be accelerated. Other research has shown that ultrasonic vibrations can alter a material (Ref. 21, 22) both during and after application of ultrasonic excitations. Additional analysis of the interface is required to determine the composition of the alloy zone.

While NiTi in the alloy zone is affected by the USS process and likely behaves differently than the bulk NiTi, it is believed that this region is sufficiently small as to not adversely affect the shape memory effect in the joined NiTi piece as mechanical constraint by the joint will cause restriction of the NiTi component on a larger scale. For that reason, the significance of the alloy zone would be in determining its effect on joint strength rather than NiTi behavior in terms of the shape memory or pseudoelastic effects.

Concluding Remarks

This paper shows that USS is a viable process for joining NiTi to Al 2024 with lap joints having an average ultimate shear strength of 7.80 ksi (53.8 MPa), and tube and socket joints having an average ultimate torsional shear strength of 5.35 ksi (36.9 MPa). The low coefficients of variance for both joint sets indicate that USS is a robust process that produces joints of consistent strength.

The residual stresses in each joint type as a result of the USS process were examined and quantified. In considering the residual stresses from soldering and shear stresses applied in testing, the von Mises equivalent stresses were found to be 13.89 ksi (96.39 MPa) for the lap shear joints and 29.15 ksi (201.0 MPa) for the torsional shear joints. Equivalent stresses show that the lower ultimate shear strength of the torsional joints is likely due to higher residual stresses present as a result of different thermal expansion coefficients of NiTi and Al 2024. However, additional modeling that incorporates the unique behavior of NiTi is required to more accurately estimate the equivalent stresses in the two types of solder joints.

Hardness mapping revealed that NiTi is generally unaffected by the USS process. This indicates that USS tempera-

tures are too low to develop a HAZ, and thereby should have no effect on the shape memory effect due to loss of material training. A thin region 6.4 μm (250 μin.) thick adjacent to the solder/NiTi interface was found to have significantly increased hardness relative to the bulk NiTi. This is believed to be due to diffusion and alloying of the filler metal and NiTi. Microcharacterization is required to determine the nature of the alloying occurring in this region. Further, the scale of the affected zone is small and any reduction in the shape memory effect of the NiTi components will be due more in part to mechanical constrain of the joint rather than the observed affected region.

The shear-based joints characterized in this paper can be geometrically optimized to take full advantage of the large transformation strains available from the NiTi components. In considering the tube and socket joints, the solder can support more torque if the shear area is increased by making deeper sockets. This will enable full detwinning of the NiTi components at the expense of the active length of the NiTi tube as more NiTi is mechanically constrained by the longer joint. An acceptable compromise between the joint strength and the amount of constrained NiTi will vary for different applications.

Acknowledgments

The authors would like to thank The Boeing Company, particularly Jim Mabe and Tad Calkins, working through the Smart Vehicle Concept Center (*www.SmartVehicleCenter.org*), a National Science Foundation Industry/University Cooperative Research Center (I/UCRC), for its technical and financial support of this research. The authors also thank Tim Frech from the Edison Welding Institute for assistance in creating the USS samples, Suresh Babu and Tapasvi Lolla from The Ohio State University Department of Materials Science and Engineering for assistance with hardness measurements, and the Smart Vehicle Concepts Graduate Fellowship Program for support of R. H.

References

1. Johnson, M. 2011. Nitinol Technical Specifications: Transformation, Physical, Electrical, Magnetic and Mechanical. *http://jmmedical.com*.

2. Weinert, K., and Petzoldt, V. 2004. Machining of NiTi based shape memory alloys. *Materials Science and Engineering* A 378: 180–184.

3. Wu, M. 2001. Fabrication of Nitinol materials and components. *Materials Science Forum* 394–395: 285–292.

4. Wang, G. 1997. Welding of Nitinol to stainless steel. *Proceedings of the International Conference on Shape Memory and Superelastic Technologies*. pp. 131–136. SMST Society, Inc.

5. Hall, P. 2005. Method of Welding Titanium and Titanium Based Alloys to Ferrous Metals. U.S. patent 6875949.

6. American Welding Society. 2007. *Brazing Handbook*. pp. 2–24, American Welding Society, Miami, Fla.

7. Vianco, P. 1999. *Soldering Handbook*. pp. 1–310, American Welding Society, Miami, Fla.

8. Hall, P. 2003. Soldering alloy. U.S. patent 6659329.

9. Zhu, L., Fino, J., and Pelton, A. 2003. Oxidation of Nitinol. *Proceedings of the International Conference on Shape Memory and Superelastic Technologies*. Eds. A. R. Pelton and T. Duerig, pp. 357–366. SMST Society, Inc.

10. Srinivasan, S. 2010. EWI Sonicsolder. *www.ewi.org*.

11. Smith, R., and Redd, R. 2006. Active solder joining of thermal management and electronic packaging. *Proceedings of the 3rd International Brazing and Soldering Conference*. pp. 79–82. ASM International.

12. ALCOA Mill Products, Inc. 2009. Alloy 2024 sheet and plate. *www.millproducts-alcoa.com.*

13. Allen, B. 1969. *Soldering Handbook: A Practical Manual for Industry and the Laboratory*. Iliffe Books Ltd.

14. Zimprich, P., Betzwar-Kotas, A., Khatibi, G., Wiess, B., and Ipser, H. 2008. Size effects in small scaled lead-free solder joints. *Journal of Materials Science: Materials in Electronics* 19(4): 383–388.

15. Hahnlen, R., and Dapino, M. 2009. Joining of shape memory NiTi to structural materials using ultrasonic soldering. *Proceedings of the ASME 2009 Conference on Smart Materials, Adaptive Structures and Intelligent Systems*. pp. 343–351. ASME.

16. Young, W., and Budynas, R. 2002. *Roark's Formulas for Stress and Strain*. 43–539, New York: McGraw-Hill.

17. Lagoudas, D., and Hartl, D. 2008. Thermomechanical characterization of shape memory alloy materials. *In Shape Memory Alloys*. Ed. D. Lagoudas, 53–120, New York, Springer Science and Business Media, LLC.

18. Kaufman, J. 2004. Aluminum alloy database. Knovel. *www.knovel.com*.

19. Dynalloy, Inc. 2008. FAQ-Flexinol Nitinol actuator wire. *www.dynalloy.com.*

20. Alapati, S., Brantley, W., Nusstein, J., Daehn, G., Svec, T., Powers, J., Johnston, W., and Gou, W. 2006. Vickers hardness investigation of work-hardening in used NiTi rotary instruments. *Journal of Endodontics* 32(12): 1191–1193.

21. Siddiqa, A., and Ghassemieh, E. 2008. Thermomechanical analyses of ultrasonic welding process using thermal and acoustic softening effects. *Mechanics of Materials* 40(12): 982–1000.

22. Schick, D. 2009. Characterization of aluminum 3003 ultrasonic additive manufacturing. MS thesis. The Ohio State University, Columbus, Ohio.